







## Atlas Review

# Characterising polymyalgia rheumatica on whole-body $^{18}\text{F}$ -FDG PET/CT: an atlas

Claire E. Owen <sup>1,2,\*</sup>, Aurora M. T. Poon<sup>3</sup>, Bonnia Liu<sup>1</sup>, David F. L. Liew <sup>1,2</sup>, Lee Pheng Yap<sup>4</sup>, Victor Yang <sup>1</sup>, Jessica L. Leung<sup>1,2</sup>, Christopher R. McMaster <sup>1,2</sup>, Andrew M. Scott<sup>2,3,5</sup>, Russell R. C. Buchanan<sup>1,2</sup>

<sup>1</sup>Department of Rheumatology, Austin Health, Heidelberg, Victoria, Australia

<sup>2</sup>Department of Medicine, University of Melbourne, Parkville, Victoria, Australia

<sup>3</sup>Department of Molecular Imaging and Therapy, Austin Health, Heidelberg, Victoria, Australia

<sup>4</sup>Department of Radiology, Austin Health, Heidelberg, Victoria, Australia

<sup>5</sup>Olivia Newton-John Cancer Research Institute and School of Cancer Medicine, La Trobe University, Melbourne, Victoria, Australia

\*Correspondence to: Claire E. Owen, Rheumatology Department, Austin Health–Repatriation Campus, Level 1, North Wing, 300 Waterdale Road, Heidelberg VIC 3084, Australia. E-mail: claire.owen@austin.org.au

## Abstract

The impact of modern imaging in uncovering the underlying pathology of PMR cannot be understated. Long dismissed as an inflammatory syndrome with links to the large vessel vasculitis giant cell arteritis (GCA), a pathognomonic pattern of musculotendinous inflammation is now attributed to PMR and may be used to confirm its diagnosis. Among the available modalities,  $^{18}\text{F}$ -fluorodeoxyglucose ( $^{18}\text{F}$ -FDG) PET/CT is increasingly recognized for its high sensitivity and specificity, as well as added ability to detect concomitant large vessel GCA and exclude other relevant differentials like infection and malignancy. This atlas provides a contemporary depiction of PMR's pathology and outlines how this knowledge translates into a pattern of findings on whole body  $^{18}\text{F}$ -FDG PET/CT that can reliably confirm its diagnosis.

## Lay Summary

PMR is the most common inflammatory rheumatic disease of older people. It typically causes disabling pain and stiffness in affected individuals at the shoulders and hips. Until recently, the precise cause for these symptoms was poorly understood. Modern scans using whole-body PET/CT (an advanced imaging test that shows where inflammation is in the body) and MRI have now identified characteristic muscle and tendon inflammation around the shoulder and hip joints, in addition to other features within the spine and at the knees and wrists/hands. This unique appearance has resulted in increasing use of PET/CT to aid PMR diagnosis in everyday clinical practice and research settings. These major advances in our knowledge are highlighted in this atlas, alongside typical examples of PMR's appearance on whole-body PET/CT.

**Keywords:** polymyalgia rheumatica, imaging, whole-body positron emission tomography/computed tomography, pathology, diagnosis.

### Key messages

- PMR is a common, chronic rheumatic disease that causes inflammation of musculotendinous structures.
- A pattern of findings throughout the whole body is characteristic of PMR on  $^{18}\text{F}$ -FDG PET/CT.
- Whole-body  $^{18}\text{F}$ -FDG PET/CT should be considered the new gold standard investigation for PMR diagnosis.

## Introduction

In the past decade, PMR, a common rheumatic entity characterized clinically by profound shoulder and hip girdle pain and stiffness, has undergone somewhat of a renaissance courtesy of advances in imaging technology. Long described as a vague inflammatory syndrome, the condition's unique musculotendinous pathology is now indisputable [1]. This development has also made it possible to definitively confirm a PMR diagnosis on imaging rather than relying solely upon clinician judgement. Previously this proved a source of

frustration for primary care providers and rheumatologists alike, particularly when assessing patients presenting with atypical features or those seemingly failing to respond to usual therapies. Among the available imaging modalities,  $^{18}\text{F}$ -fluorodeoxyglucose ( $^{18}\text{F}$ -FDG) PET/CT has emerged as the logical gold standard investigation, owing to its unique ability to document PMR's characteristic whole-body pathology, detect concomitant large vessel giant cell arteritis (LV-GCA) and exclude relevant differential diagnoses including

Received: 7 October 2023. Accepted: 12 December 2023

© The Author(s) 2024. Published by Oxford University Press on behalf of the British Society for Rheumatology.

This is an Open Access article distributed under the terms of the Creative Commons Attribution-NonCommercial License (<https://creativecommons.org/licenses/by-nc/4.0/>), which permits non-commercial re-use, distribution, and reproduction in any medium, provided the original work is properly cited. For commercial re-use, please contact [journals.permissions@oup.com](mailto:journals.permissions@oup.com)

infection and malignancy [2]. Although radiation exposure, cost and availability represent certain barriers to the routine use of PET/CT for PMR diagnosis, its utility in circumstances of diagnostic uncertainty and, potentially, to ensure the homogeneity of clinical trials populations is clear. In the following atlas, a modern interpretation of PMR's underlying pathology based on imaging insights is provided, together with examples of hallmark findings that may be detected by whole-body  $^{18}\text{F}$ -FDG PET/CT.

## Imaging and its role in revealing the pathology of PMR

The first report of PMR in the medical literature is attributed to Dr William Bruce in 1888, however, it took another century before imaging, in the form of ultrasound, was employed to help characterize its pathology [3, 4]. Early biopsy studies ultimately failed to account for the severity of pain and stiffness experienced by PMR patients at the shoulder and hip girdle, with a mild synovitis documented at the glenohumeral joint and no discernible abnormality of muscle fibres on histopathology (although oedema and perivascular chronic inflammatory cell infiltration of the muscular fascia and its tendinous septum were described) [5, 6]. In 1999, Cantini *et al.* [7] found a significantly higher frequency of subacromial bursitis among PMR patients compared with cases of elderly-onset RA but no difference in their respective rates of synovitis/joint effusion or biceps tenosynovitis. Evidence for an extracapsular predominant pattern of inflammation to distinguish PMR from RA was subsequently confirmed using shoulder MRI [8].

While early PET work documented increased  $^{18}\text{F}$ -FDG uptake at the shoulders and hips of PMR patients, it was not until the advent of hybrid technology with low-dose CT that distinct anatomical structures could be accurately correlated [9]. Accordingly, key differences in the distribution of abnormal findings in PMR as compared with RA and SpA have become increasingly apparent, including the highly specific presence of cervical and/or lumbar interspinous involvement and pathognomonic intense  $^{18}\text{F}$ -FDG avidity adjacent to the ischial tuberosities [10]. While both these findings were previously attributed to bursitis, the latter has since been demonstrated to correspond to hamstring peritendonitis on PET/MRI fusion [11]. Indeed, work by Fruth *et al.* [12] using contrast-enhanced pelvic MRI proved tendinous structures as the precise anatomic correlate of extracapsular inflammation in PMR, the pathology ranging from 'circumferential peritendinous inflammation to complete intratendinous involvement up to the level of the musculotendinous junction'. The discovery of myofascial inflammatory lesions (described as high T2 short-tau inversion recovery signal within the affected muscle or forming a line around it) at the shoulder and/or pelvic girdle among all participants in the landmark Tocilizumab Effect in Polymyalgia Rheumatica (TENOR) study has since confirmed that PMR's pathology can also extend into the adjacent muscle perimysium; a notable finding, considering historical histopathology recording inflammatory infiltration of the muscle fascia [6, 13].

Such imaging insights have effectively demystified the pathology of PMR. Increasingly, it seems that the connective tissues surrounding the muscle and its adjacent tendon, specifically the contiguous perimysium and peritendon, represent the target antigen of autoimmunity in this rheumatic

disease. Involvement of adjacent structures, including the bursa, which sit between tendons at large joints to prevent friction, and the underlying joint capsule and ligaments is also typical. Clinically, the result is extreme limitation of movement at the glenohumeral and coxofemoral joints, together with painful impingement due to subacromial bursitis at the shoulders and discomfort localizing to key musculotendinous sites including biceps brachii and the origin (adjacent to the ischial tuberosities) and insertion (at the posteromedial knee) of the hamstring muscles. In Figs 1 and 2, a modern depiction of PMR's pathology at the peri-articular shoulder and posterior hip and knee is provided.

## Utilising whole-body $^{18}\text{F}$ -FDG PET/CT to detect PMR's distinctive pathology

Although the combination of functional and anatomic imaging offered by PET/CT was developed for evaluating malignancies, the value of co-registration for the diagnosis and monitoring of inflammatory conditions is similarly clear [14]. Blockmans *et al.* [15] first noted the presence of abnormal  $^{18}\text{F}$ -FDG uptake at the shoulder and hip joints among GCA patients undergoing PET to assess for the presence of large vessel vasculitis (LVV). Later work in a dedicated PMR population documented a novel finding at the processi spinosi, now referred to in the literature as interspinous uptake/involvement [9]. As alluded to, although PET/CT involves radiation exposure and is subject to certain practical limitations, its capacity to document this distinctive extracapsular pathology throughout the whole body is unrivalled. This is of particular importance given that isolated musculoskeletal findings on imaging have consistently proven insufficient for making a reliable PMR diagnosis; when developing the optional ultrasound component of the 2012 EULAR/ACR Classification Criteria, only the combination of abnormalities at both shoulders, or one shoulder and one hip, proved sufficient to improve specificity [16]. Similarly, while the superior resolution and depth of MRI offers the advantage over ultrasound of detecting other characteristic features like peritendonitis and myofascial inflammation, this modality is otherwise limited to evaluating a single musculoskeletal region at a time and consequently cannot simultaneously assess for concomitant LV-GCA or exclude other relevant differentials.

### Peri-articular $^{18}\text{F}$ -FDG uptake at the shoulders and hips including the trochanteric regions

With knowledge of PMR's unique predilection for muscle tendon, its fascia and the adjacent bursae and joint capsule, it stands to reason that a peri-articular distribution of abnormal  $^{18}\text{F}$ -FDG uptake is characteristically observed at the shoulders and hips on PET/CT (Figs 3–5). Anterior to the glenohumeral joint, a discrete area of  $^{18}\text{F}$ -FDG avidity can be seen corresponding to the long head of the biceps tendon, with involvement near the distal insertion at the elbow also appreciated in some instances (Fig. 6). This may account for the common report by patients of pain coursing down the arm into the elbow joint. Similarly, at the hip, intensities adjacent to the origins and insertions of muscle groups around the coxofemoral joints can be appreciated. The bursae of both the shoulder and trochanteric regions notably comprise numerous synovial membrane-lined sacs, positioned between muscles, tendons, ligaments and bones to minimize friction

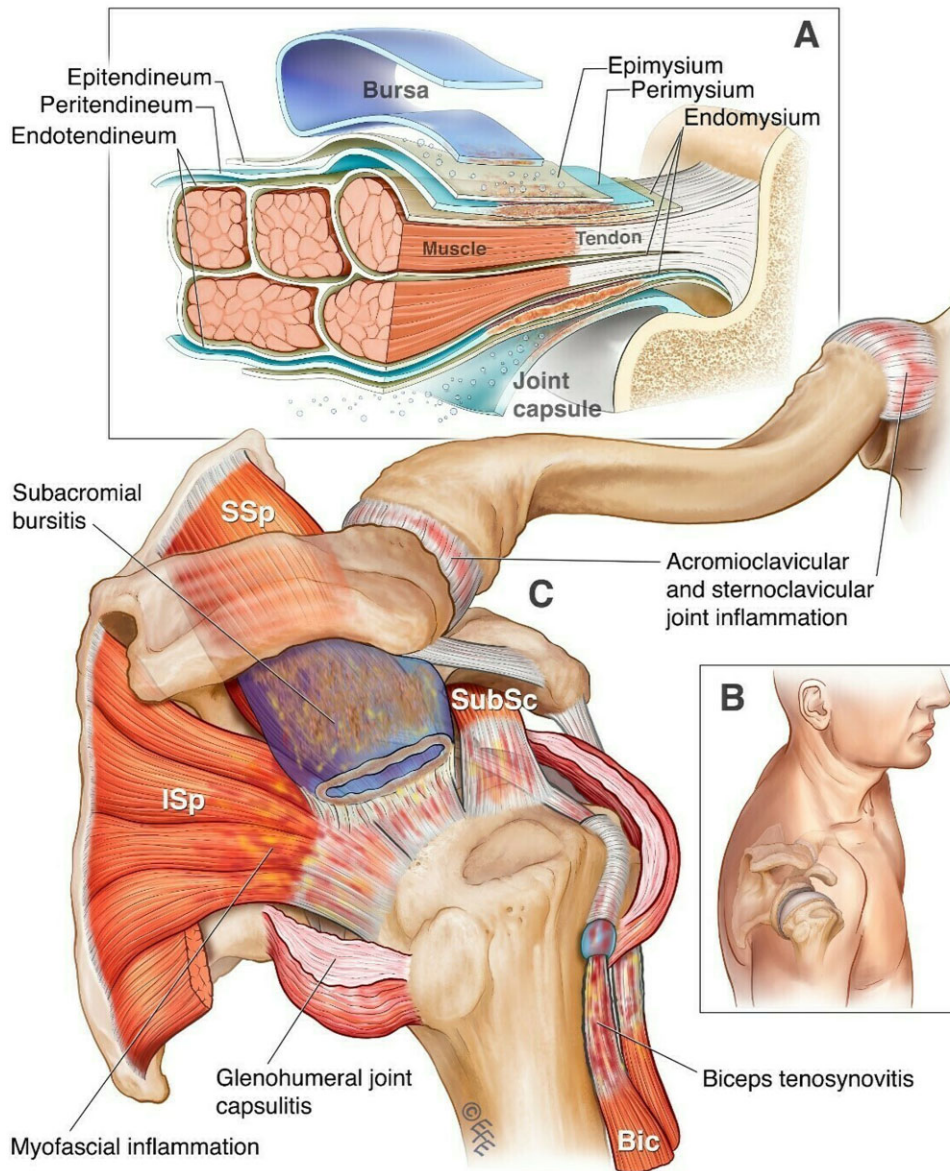


**Figure 1.** PMR's pathology at the peri-articular shoulder. **(A)** A depiction of inflammation arising from the connective tissues of the tendons and muscles (peritendineum and perimysium) to involve adjacent structures including the bursa and joint capsule. **(B)** A posteromedial view of the shoulder for anatomical orientation. **(C)** Distinctive musculotendinous manifestations of PMR at the shoulder. Bic: biceps brachii; Isp: infraspinatus; SSp: supraspinatus; SubSc: subscapularis. © Dr Levent Efe, CMI

and permit free movement of the underlying large joint [17]. Not surprisingly, such structures are not clearly apparent at the image resolution offered by low-dose CT.

A peri-articular pattern of abnormal  $^{18}\text{F}$ -FDG uptake should be visualized at the shoulder and/or hip girdle in every PMR patient. While normal controls may demonstrate abnormalities in a similar distribution, corresponding to degenerative tendinopathy at the same musculotendinous structures, the extent is far greater and the  $^{18}\text{F}$ -FDG avidity recorded by objective measures like the maximum standardised uptake value ( $\text{SUV}_{\text{max}}$ ) significantly higher among PMR cases [10]. In particular, bilateral low-grade trochanteric uptake is often appreciated on PET/CT in older adults and hence possesses insufficient specificity for a PMR diagnosis.

Intra-articular abnormalities are still commonly detected among PMR patients at the shoulders and hips, however, such findings fail to distinguish PMR from other

inflammatory conditions, like RA and SpA [10]. However, involvement of the sternoclavicular joints is an exception to this rule, with intense  $^{18}\text{F}$ -FDG avidity at these sites noted for their high specificity to PMR [2]. Abnormalities at the sternoclavicular joints have accordingly been included in several PET/CT scoring systems developed to aid PMR diagnosis.

### Interspinous involvement

Between the cervical and lumbar interspinous processes, abnormal  $^{18}\text{F}$ -FDG uptake is frequently observed in PMR. This finding has consistently been demonstrated to be a highly specific imaging feature in the literature [2, 10, 18, 19]. Salvarani *et al.* [20, 21] first investigated the anatomic correlate of PET anomalies in the cervical and lumbar spine using MRI, documenting cervical interspinous bursitis in all PMR patients scanned and lumbar interspinous bursitis in 9/10

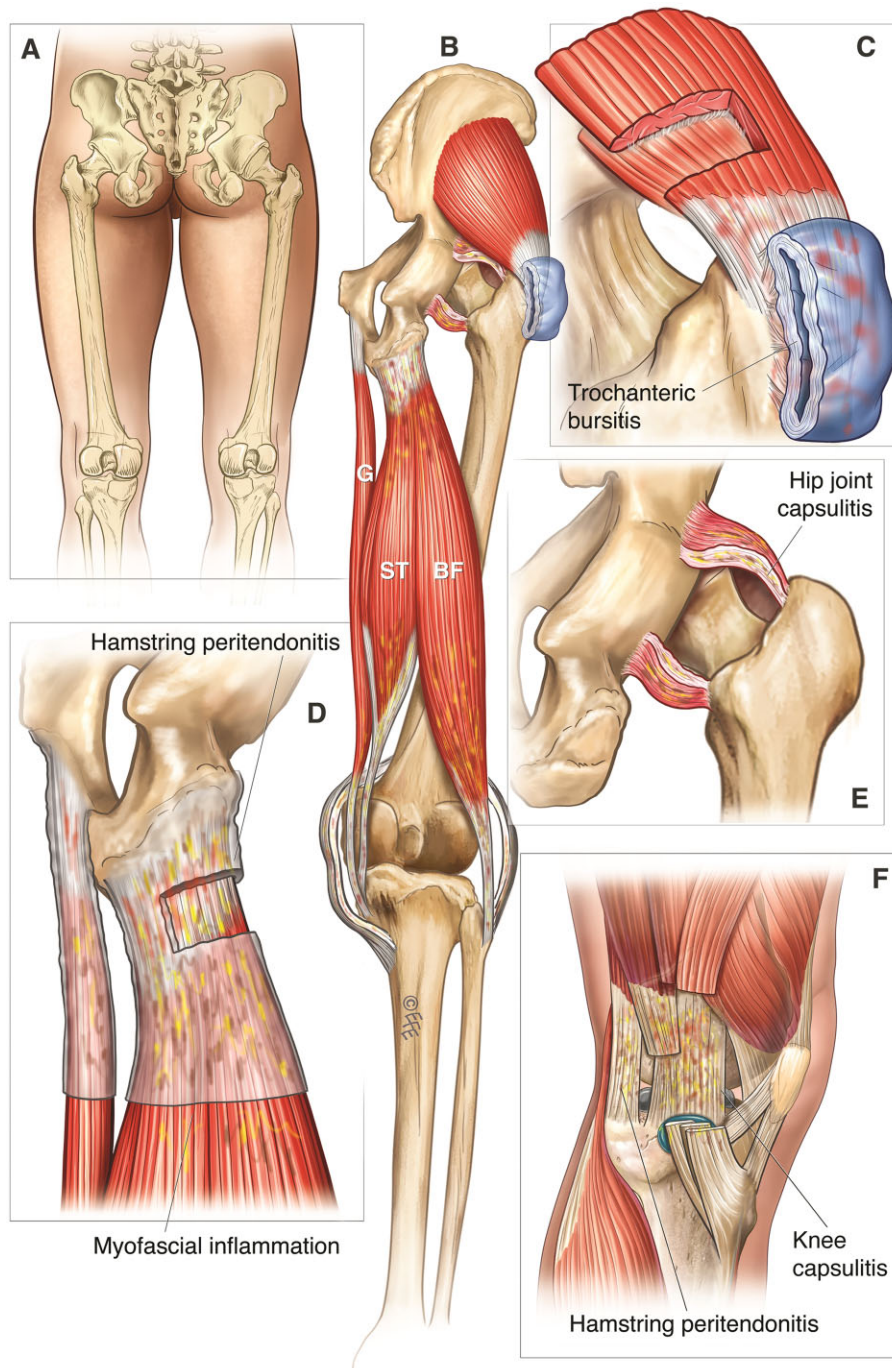


**Figure 2.** PMR's pathology at the posterior hip and knee. (A) A posterior view of the hip and knee joints for anatomical orientation. (B–F) Distinctive musculotendinous manifestations of PMR at the hip and knee. BF: biceps femoris; G: gracilis; ST: semitendinosus. © Dr Levent Efe, CMI

cases. In this instance, however, the interspinous bursa is not a synovial membrane-lined sac positioned between musculoskeletal structures, but adventitial—a potential space that develops due to local mechanical factors, specifically a small interspinous distance relative to the height of the vertebral body ('the bursal index') [17, 22]. These bursae typically consist of narrow slits arising from the base of the spinous process below, extending up from the dorsal surface of the ligamentum flavum to the underside of the spinous process above [23]. On histology, mucoid and myxomatous degeneration of surrounding connective tissues is noted, with comparatively few synovial cells seen [22, 24].

Like elsewhere in the body, improved imaging technology has enabled better anatomical correlation of interspinous  $^{18}\text{F}$ -FDG uptake. Consequently, it is now established that two distinct patterns may be observed on PET/CT in the interspinous regions: focal, due to interspinous bursitis, and diffuse, hypothesized until now to arise from interspinous ligament inflammation. In Fig. 7 we present MRI correlation confirming ligamentous inflammation as the aetiology of a diffuse pattern of abnormal  $^{18}\text{F}$ -FDG uptake between the interspinous processes. As previously suggested, and in keeping with the model of pathology presented at the beginning of this atlas, chronic ligamentous inflammation due to PMR may lead to interspinous

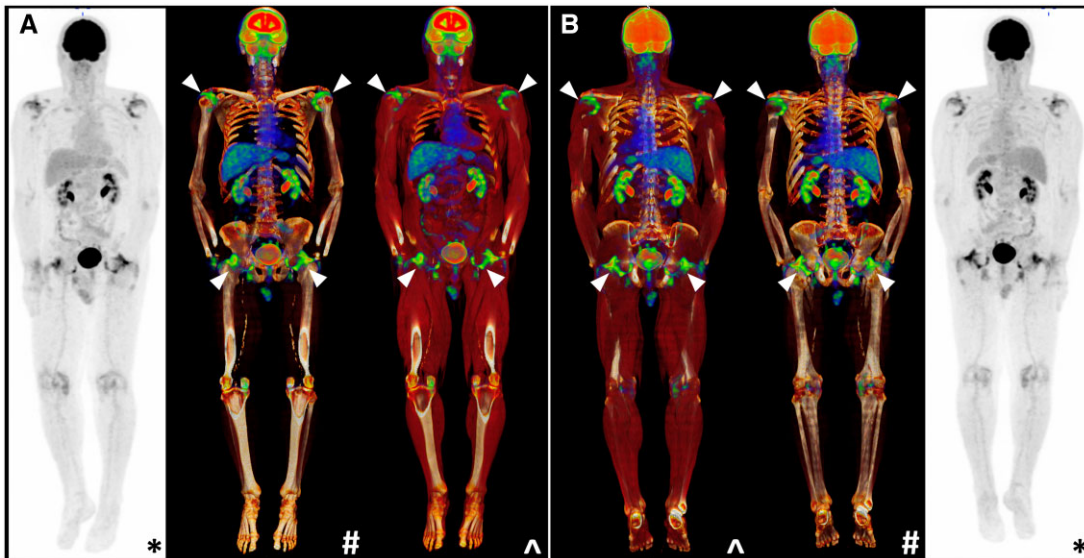


**Figure 3.** Characteristic peri-articular  $^{18}\text{F}$ -FDG uptake on PET/CT at the shoulders and hips in a PMR patient (white arrows). Whole-body coronal views are provided from an (A) anterior and (B) posterior aspect. \*Maximal intensity projection (MIP); #CT windowing with bone only; ^CT windowing with muscle and bone

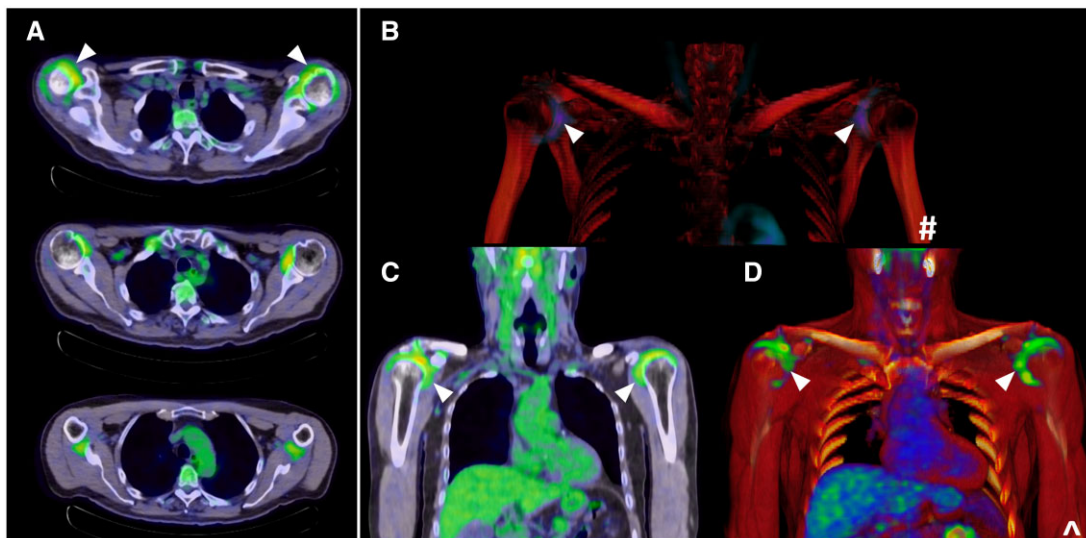


**Figure 4.** Shoulder involvement on PET/CT in PMR: abnormal  $^{18}\text{F}$ -FDG uptake (white arrows) at the shoulders appreciated in (A) sequential axial views and (B–D) coronal views

bursa formation and the development of bursitis, which can be detected by whole-body PET/CT.

### $^{18}\text{F}$ -FDG uptake adjacent to the ischial tuberosities and at the posteromedial knee

Posterior thigh pain behind the knee and into the calf region is a common complaint among PMR patients. On PET/MRI fusion, intense  $^{18}\text{F}$ -FDG uptake adjacent to the ischial tuberosities (Fig. 8) is known to correspond to peritendonitis of the hamstring tendons, specifically the semimembranosus and the long head of the biceps femoris, at their common origin. Given their size relative to other PMR-affected musculotendinous structures, it is unsurprising that this site consistently records the highest mean  $\text{SUV}_{\text{max}}$  throughout the whole body.

At the knee, a peri-articular pattern of abnormal uptake analogous to the shoulder and hip joints is similarly observed

in the majority of PMR patients (Fig. 8) [25]. Noted to correlate anatomically with the contour of the fibrous joint capsule by Cimmino *et al.* [11], this work also documented focal areas of  $^{18}\text{F}$ -FDG avidity in a posteromedial distribution, which have since been attributed to peritendonitis of the distal semitendinosus and gracilis muscles that insert via the pes anserinus at the medial tibial condyle. Given praepubic uptake on PET/CT has also been reported in the PMR literature, it stands to reason that the tendon of the gracilis muscle as it arises from the pubic symphysis may also be affected, together with adjacent hip adductors [26].

### Wrist and hand involvement

In the PMR literature, there is no more contentious issue than that of peripheral arthritis. For some rheumatologists, pain and swelling at the wrists and/or hands still mandates a

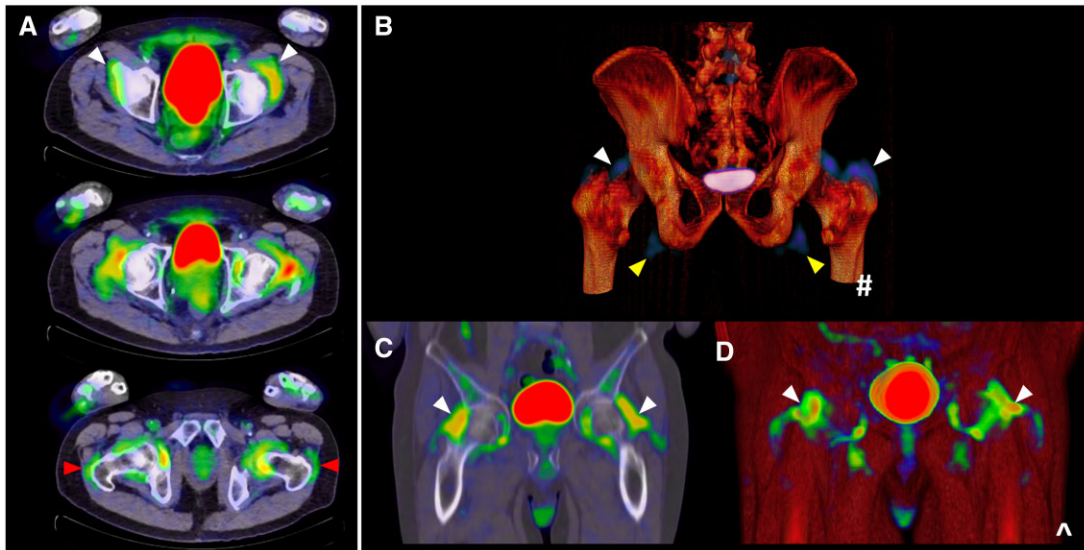


**Figure 5.** Hip involvement on PET/CT in PMR: abnormal  $^{18}\text{F}$ -FDG uptake (white arrows) at the hips appreciated in **(A)** sequential axial views, including at the trochanteric regions (red arrows), and **(B-D)** coronal views, with yellow arrows also indicating  $^{18}\text{F}$ -FDG avidity adjacent to the ischial tuberosities

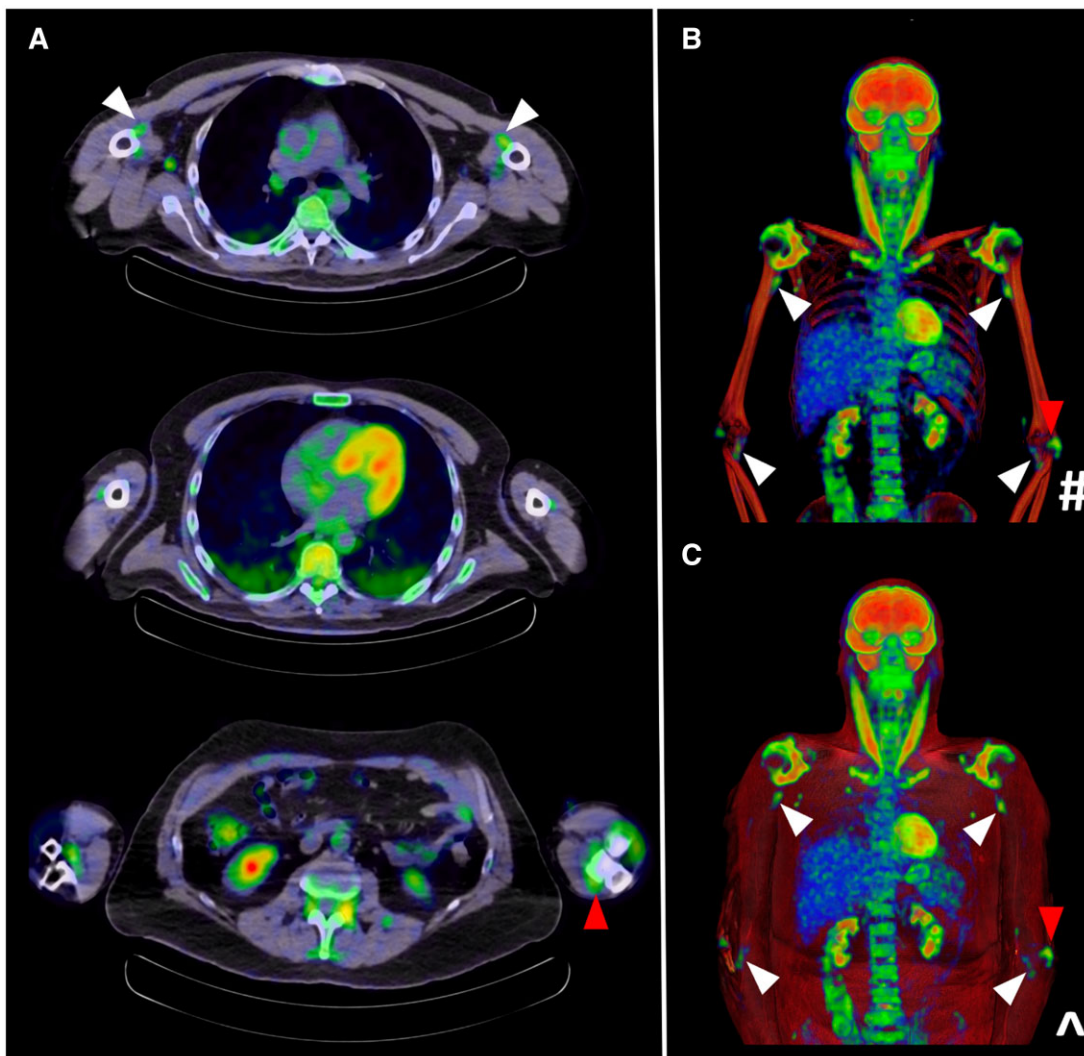


**Figure 6.** Biceps involvement on PET/CT in PMR: **(A)** sequential axial views tracking the biceps down the arm to the elbow (white arrows);  $^{18}\text{F}$ -FDG avidity of the distal triceps is also appreciated in the olecranon fossa (red arrow); **(B, C)** coronal views

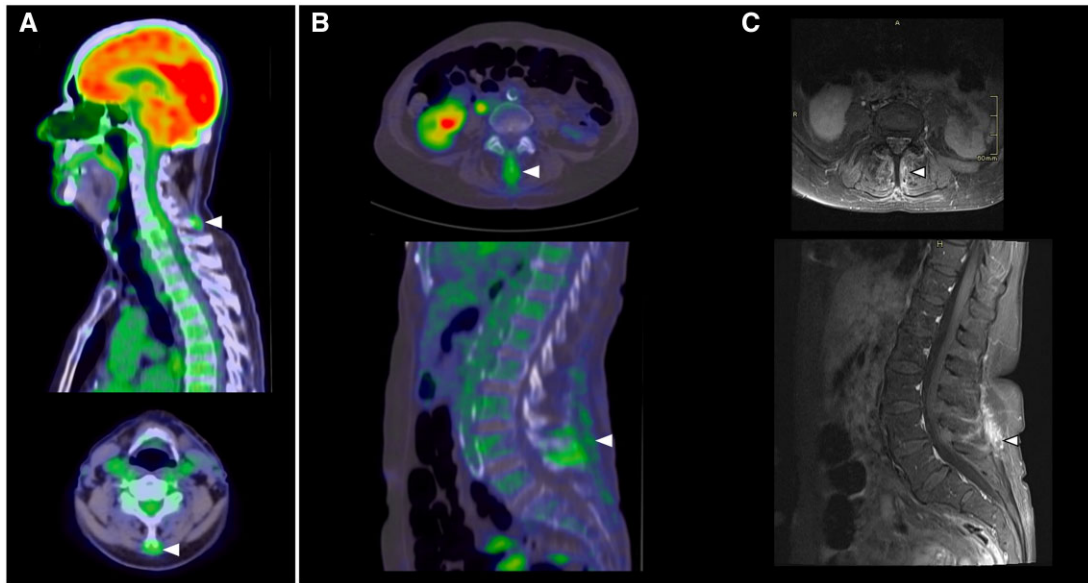


**Figure 7.** Interspinous involvement on PET/CT in PMR: abnormal  $^{18}\text{F}$ -FDG uptake (white arrows) at (A) the cervical spine and (B) the lumbar spine. (C, D) Correlation of lumbar spine findings on T1-weighted fat saturated (T1FS) post-contrast MRI demonstrating interspinous and supraspinous ligament enhancement at L4–5

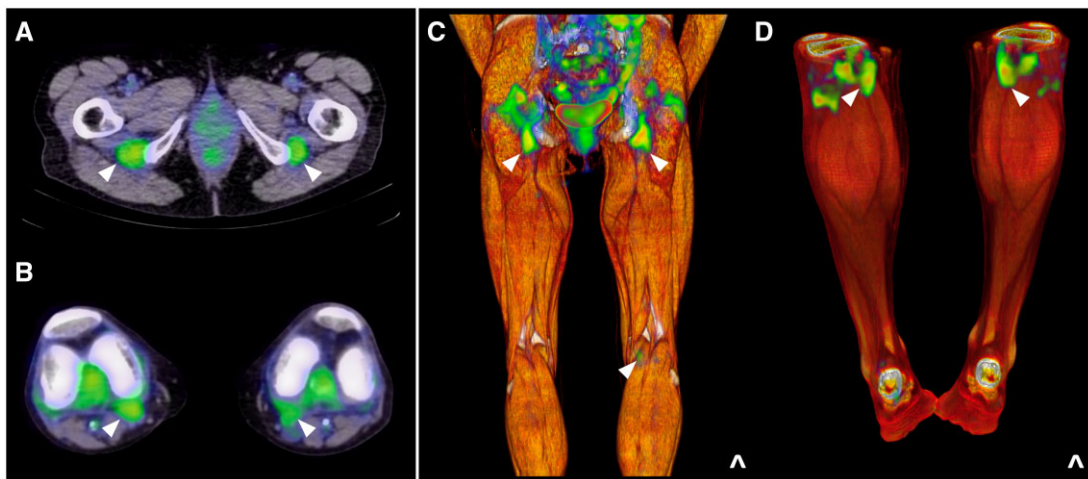


**Figure 8.** Hamstring involvement on PET/CT in PMR: abnormal  $^{18}\text{F}$ -FDG uptake (white arrows) adjacent to (A) the ischial tuberosities and at (B) the posteromedial knee; (C, D) coronal views

change in classification to late-onset seronegative RA. From both a clinical and imaging standpoint though, this approach is not evidence-based, with almost one-half of patients experiencing symptoms in this distribution and a similar proportion exhibiting abnormal  $^{18}\text{F}$ -FDG uptake using dedicated hand views on whole-body PET/CT [11, 27]. Both joint-based and volar patterns can be observed, the latter corresponding to the presence of flexor tenosynovitis (Fig. 9). This is of particular significance, given MRI studies have established an extracapsular distribution of inflammation at the metacarpophalangeal joints as a key differentiator between PMR and RA, while a much higher incidence of tenosynovitis has been documented among PMR patients compared with normal controls [28, 29].

Remitting seronegative symmetrical synovitis with pitting oedema (RS3PE) syndrome describes a clinical entity characterized by an exquisitely steroid-responsive polysynovitis of the hands and/or feet that occurs in association with swelling

of the extremities [30]. Originally considered a distinct subset of seronegative RA, RS3PE has since been reported in association with a range of rheumatic conditions, including PMR. Given tenosynovial sheath inflammation represents the imaging hallmark of this presentation, with concomitant joint synovitis also present in some cases, RS3PE syndrome represents another example of musculotendinous pathology that may be seen as part of PMR's disease spectrum.

#### Concomitant LV-GCA

Approximately one in five PMR patients will have concomitant GCA, although up to 50% of GCA cases experience musculoskeletal symptoms of PMR [31]. In a recent meta-analysis, the pooled prevalence of subclinical LV-GCA across 13 studies comprising 566 steroid-naïve participants was 23%, although this figure was higher (29%) when PET/CT was utilized as the screening method ( $n = 266$  patients) [32]. A diffuse and linear pattern of abnormal  $^{18}\text{F}$ -FDG uptake is

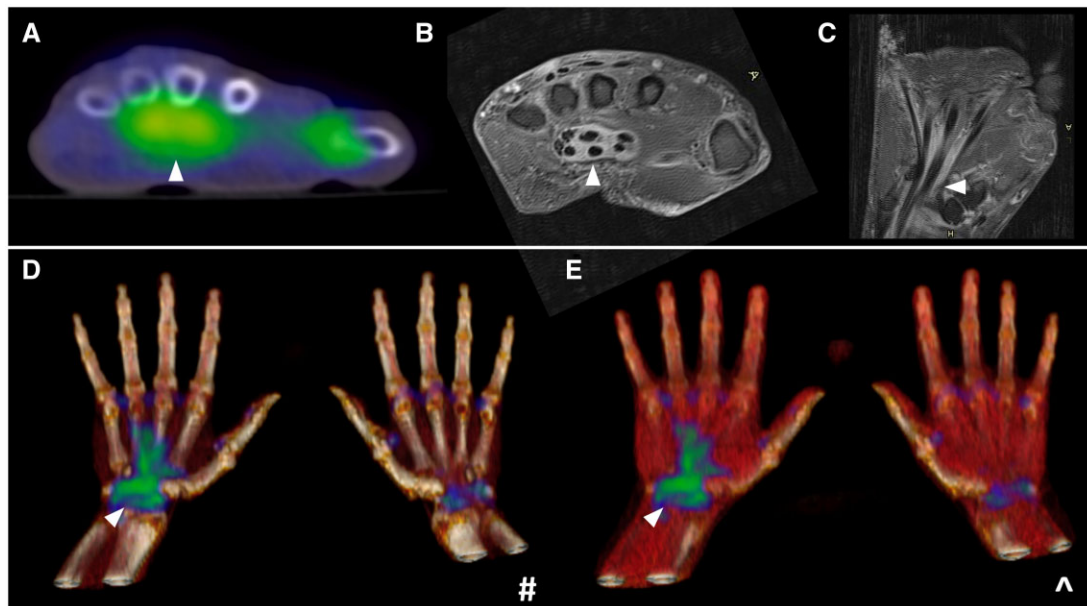


**Figure 9.** Hand involvement on PET/CT in PMR: **(A)** a volar pattern of abnormal  $^{18}\text{F}$ -FDG (white arrows) uptake at the hand; **(B)** confirmation of flexor tenosynovitis as the corresponding abnormality on T1FS post-contrast MRI; **(C-E)** coronal views

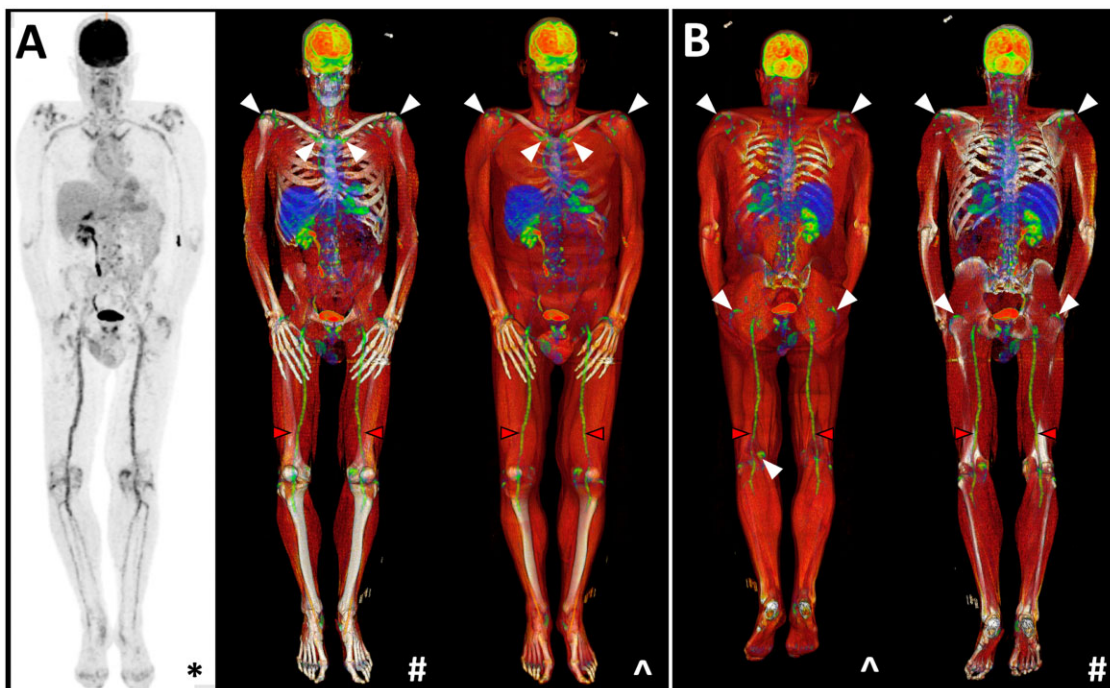


**Figure 10.** Concomitant LV-GCA (red arrows) detected on PET/CT in a PMR patient with characteristic involvement of the peri-articular shoulders and hips, sternoclavicular joints and left posteromedial knee (white arrows). \*Maximal Intensity projection (MIP); #CT windowing with bone only; ^CT windowing with muscle and bone

characteristic of LVV (Fig. 10), with the degree of avidity equal to or higher than that observed at the liver [33]. Such findings merit institution of treatment as in confirmed cranial GCA. Sometimes, lower grade vascular abnormalities are observed in PMR patients on imaging, but their long-term significance is presently unknown and hence more aggressive management is not justified. It is apparent however that patients experiencing intractable PMR symptoms are more likely to have underlying LV-GCA [34]. A PET/CT study of 84 PMR cases found positive scan results in 60.7%, with

predictors including diffuse lower limb pain [odds ratio (OR) 8.8], pelvic girdle pain (OR 4.8) and inflammatory low back pain (OR 4.7).

### Determining the likelihood of a PMR diagnosis on whole-body $^{18}\text{F}$ -FDG PET/CT

Knowledge of PMR's distinctive pathology on PET/CT has led to further evaluation of its diagnostic potential. In Figs 11 and 12, key differences in the imaging appearance of PMR



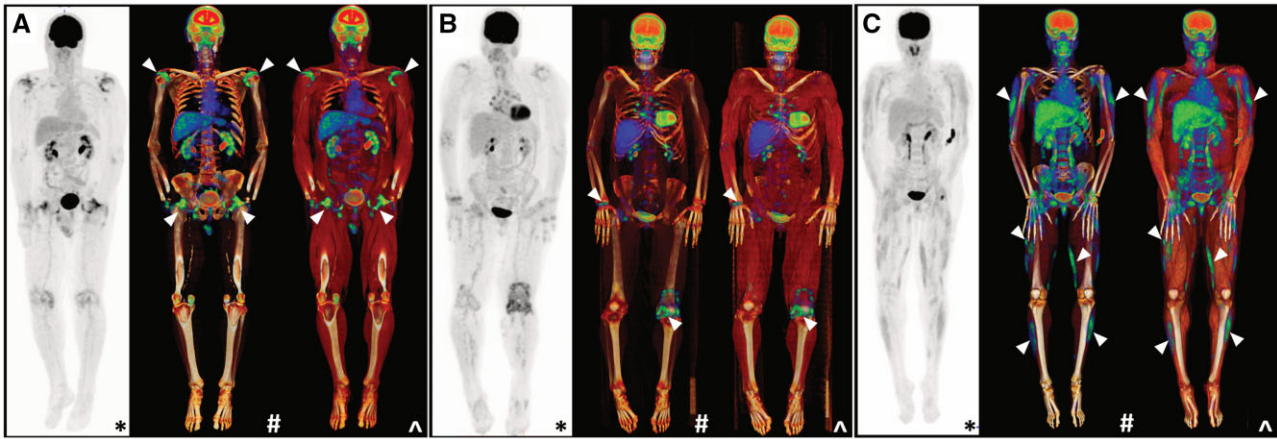


**Figure 11.** Differences in the whole-body appearance of PET/CT in (A) PMR compared with the relevant differential diagnoses of (B) seropositive RA and (C) dermatomyositis. In RA, <sup>18</sup>F-FDG avidity is appreciated in an intra-articular distribution, while in dermatomyositis, abnormalities are localized to the muscle (white arrows). \*Maximal intensity projection (MIP); #CT windowing with bone only; ^CT windowing with muscle and bone

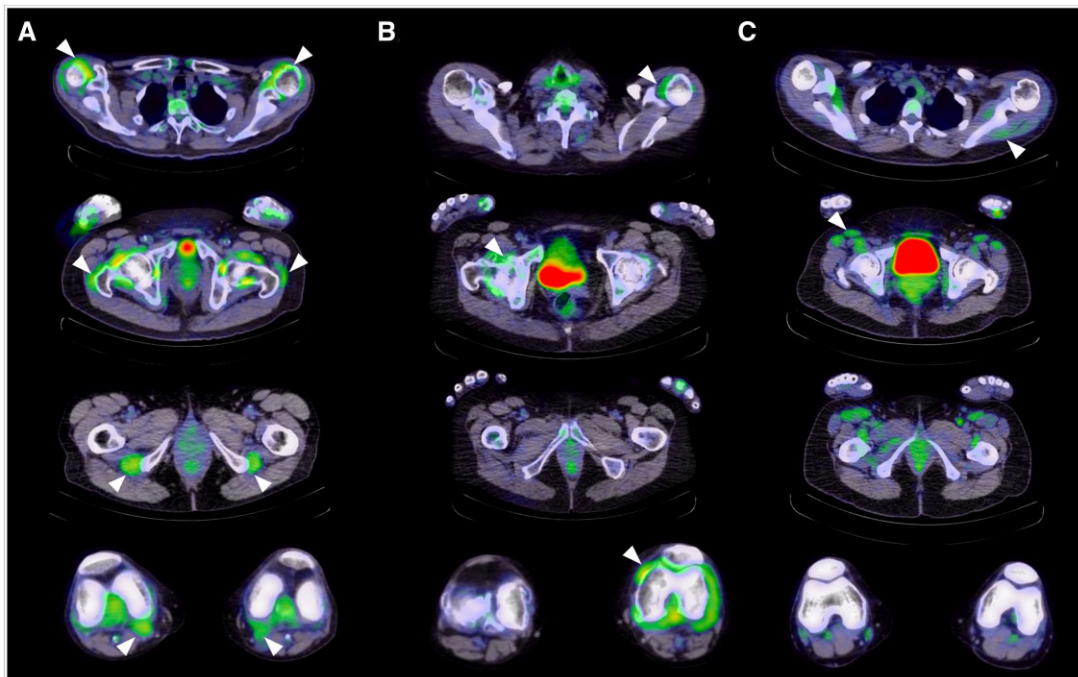


**Figure 12.** Differences in the axial appearance of <sup>18</sup>F-FDG PET/CT in (A) PMR, (B) seropositive RA and (C) dermatomyositis (white arrows). Views are taken at the level of the shoulders, hips, ischial tuberosities and knees for direct comparison

compared with seropositive RA and dermatomyositis are demonstrated. Early PET/CT studies established significant differences in the frequency of abnormalities and <sup>18</sup>F-FDG avidity between cases and normal controls, but also determined that the sensitivity and/or specificity of findings at individual musculoskeletal sites was insufficient to confirm a PMR diagnosis [18, 19]. More recent scoring approaches have therefore combined pathognomonic PET/CT findings of PMR, including abnormal <sup>18</sup>F-FDG uptake around the shoulders and hips, in the interspinous regions and adjacent to the ischial tuberosities [2, 35]. The Leuven score, which is calculated by summing the degree of <sup>18</sup>F-FDG avidity at 12 prespecified sites based on the Meller score [33], has been demonstrated to possess the best diagnostic accuracy in the

existing literature (sensitivity 91.4%, specificity 97.6%) [36]. A modified version (the Leuven/Groningen score) that limits the number of musculoskeletal sites scored to only seven has since been developed and validated, achieving comparable sensitivity and specificity [2]. In everyday clinical practice however, a simpler approach is preferred. To that end, the Heidelberg algorithm, which mandates the presence of <sup>18</sup>F-FDG uptake equal to or greater than that of the liver (Meller score  $\geq 2$  [33]) adjacent to the ischial tuberosities in combination with either the peri-articular shoulders or interspinous regions, has been proposed [10]. In an external validation exercise, this actually achieved the same sensitivity as the Leuven/Groningen score, although it had slightly less specificity (78.9%) [2].

**Table 1.** Recommended technical specifications for undertaking whole-body <sup>18</sup>F-FDG PET/CT in patients with suspected or established PMR

Specification	Recommended approach	Further details
Physical activity	Avoid strenuous activity for 24 h beforehand and during tracer uptake	
Fasting	Minimum 6 h	Limit oral intake to plain water only Ensure cessation of tube feeding, i.v. dextrose and parenteral nutrition
Blood glucose control	≤7 mmol/l	Exogenous insulin may be utilized to address hyperglycaemia [40]
<sup>18</sup> F-FDG dosage	Weight based	2–3 MBq/kg (0.054–0.081 mCi/kg)
Uptake period	60 min; 120 min has been advocated for in some studies to optimize large vessel imaging	Ensure temperature-regulated room
Position	Supine with arms by side	Avoid arms overhead to optimize shoulder imaging
Extent	Skull vertex to below the knees	Dedicated hand views may also be obtained
Expected findings	Peri-articular shoulder uptake Peri-articular hip uptake Interspinous uptake Uptake adjacent to the ischial tuberosities Posteromedial knee uptake Volar hand uptake Concomitant LV-GCA (≈20%)	

## Pitfalls to consider

Heterogeneity in the performance of <sup>18</sup>F-FDG PET/CT for the diagnosis of PMR has been previously attributed to variations in imaging protocols [35, 37]. Census procedural recommendations now outline technical aspects specific to PMR and LVV, thereby ensuring consistent interpretation of findings, as some features are common to other inflammatory conditions (e.g. RA and atherosclerosis) [38, 39]. In Table 1, the recommended protocol for PET/CT in patients with suspected or established PMR is outlined. Key factors to minimize false-negative results include appropriate fasting and blood glucose control to minimize competitive inhibition of <sup>18</sup>F-FDG, while strenuous activity should be avoided for 24 h prior to and immediately following tracer administration so that physiological muscle and brown fat uptake is limited [41, 42]. Given that a diagnosis of PMR on PET/CT is dependent upon a combination of abnormal findings, it is crucial that the field of view encompasses all relevant musculoskeletal sites. Image acquisition is recommended after a minimum uptake time of 60 min to ensure optimal target:background ratios, although several studies have advocated for longer uptake times (typically 120 min) to ensure accurate large vessel imaging and better distinguish between atherosclerosis and arteritis [38, 40, 41]. Spatial resolution and accuracy can be further improved by increasing acquisition time per bed position from 2–3 min to 8 min, however, this significantly increases the total scan duration [38, 43].

Glucocorticoid use is known to reduce the sensitivity of PET/CT, both due to treatment of the underlying inflammatory condition and its impact on physiological liver uptake, which typically provides the reference standard for grading <sup>18</sup>F-FDG uptake [18, 44]. In the LV-GCA literature, it is established that the intensity of <sup>18</sup>F-FDG decreases after just 72 h of high-dose glucocorticoid therapy, with resultant compromise in the likelihood of a PET-positive result by day 10 [45]. Comparatively little is known about the impact of prednisolone doses used to treat PMR (typically ≤15 mg/day). However, it is the experience of the authors of this atlas that while <sup>18</sup>F-FDG avidity is reduced, the distribution of uptake

on PET/CT remains consistent with that observed in steroid-naïve PMR patients. If clinically appropriate, a brief withdrawal of glucocorticoid therapy to restore pathological <sup>18</sup>F-FDG uptake can be considered, but again the evidence to support this approach is lacking.

## Conclusion and future avenues

For far too long, PMR has been the archetype of an invisible illness, causing chronic pain and disability among its many sufferers but proving difficult for health professionals to definitively diagnose and manage. Thanks to the role played by imaging in revealing its unique musculotendinous pathology, the legitimacy of PMR as a distinct disease entity is no longer in question. This atlas provides examples of characteristic findings on whole-body <sup>18</sup>F-FDG PET/CT that can reliably form the basis for a PMR diagnosis. There is no doubt that this modality represents the modern gold standard investigation for PMR, although it would be preferable to find a lower-cost imaging test with greater availability to fulfil this role in everyday clinical practice. Moving forwards, it will be key to translate the information that PET/CT has provided into meaningful change in the standard of care available to patients living with PMR. Study of the interplay between scintigraphic changes and conventional and novel biomarkers will be imperative, along with pilot evaluation of PET/CT's potential as an instrument to measure PMR disease activity and assess treatment response.

## Data availability

No new data were generated or analysed in support of this research.

## Authors' contributions

C.E.O. and D.F.L. conceptualised the manuscript. A.M.T.P. contributed all example images and C.E.O. prepared each figure. C.E.O. wrote the original draft, with contributions from authors B.L. and V.Y. L.P.Y. oversaw interpretation of

included MRI images. All authors reviewed each iteration of the manuscript to final completion.

## Funding

No specific funding was received from any bodies in the public, commercial or not-for-profit sectors to carry out the work described in this article.

*Disclosure statement:* The authors have declared no conflicts of interest.

## Acknowledgements

The authors wish to acknowledge Dr Levent Efe for the illustrations provided in Figs 1 and 2. Images utilized in this publication have been provided in accordance with Human Research Ethics Committee approval (95689/Austin-2023).

## References

- Owen CE, Liew DFL, Buchanan RRC. Musculotendinous inflammation: the defining pathology of polymyalgia rheumatica? *J Rheumatol* 2019;46:1552–5.
- van der Geest KSM, van Sleen Y, Nienhuis P *et al.* Comparison and validation of FDG-PET/CT scores for polymyalgia rheumatica. *Rheumatology (Oxford)* 2021;61:1072–82.
- Mowat AG. Strathpeffer Spa: Dr William Bruce and polymyalgia rheumatica. *Ann Rheum Dis* 40:503–6.
- Koski JM. Ultrasonographic evidence of synovitis in axial joints in patients with polymyalgia rheumatica. *Br J Rheumatol* 1992; 31:201–3.
- Meliconi R, Pulsatelli L, Uguccioni M *et al.* Leukocyte infiltration in synovial tissue from the shoulder of patients with polymyalgia rheumatica. Quantitative analysis and influence of corticosteroid treatment. *Arthritis Rheumatol* 1996;39:1199–207.
- Gordon I, Rennie AM, Branwood AW. Polymyalgia rheumatica: biopsy studies. *Ann Rheum Dis* 1964;23:447–55.
- Cantini F, Salvarani C, Olivieri I. Shoulder sonographic findings in polymyalgia rheumatica. *J Rheumatol* 1999;26:2501–2.
- McGonagle D, Pease C, Marzo-Ortega H *et al.* Comparison of extracapsular changes by magnetic resonance imaging in patients with rheumatoid arthritis and polymyalgia rheumatica. *J Rheumatol* 2001;28:1837–41.
- Blockmans D, De Ceuninck L, Vanderschueren S *et al.* Repetitive 18-fluorodeoxyglucose positron emission tomography in isolated polymyalgia rheumatica: a prospective study in 35 patients. *Rheumatology (Oxford)* 2007;46:672–7.
- Owen CE, Poon AMT, Yang V *et al.* Abnormalities at three musculoskeletal sites on whole-body positron emission tomography/computed tomography can diagnose polymyalgia rheumatica with high sensitivity and specificity. *Eur J Nuclear Med Mol Imaging* 2020;47:2461–8.
- Owen CE, Poon AMT, Lee ST *et al.* Fusion of positron emission tomography/computed tomography with magnetic resonance imaging reveals hamstring peritendonitis in polymyalgia rheumatica. *Rheumatology (Oxford)* 2018;57:345–53.
- Fruth M, Buehring B, Baraliakos X, Braun J. Use of contrast-enhanced magnetic resonance imaging of the pelvis to describe changes at different anatomic sites which are potentially specific for polymyalgia rheumatica. *Clin Exp Rheumatol* 2018;36(Suppl 114):86–95.
- Laporte JP, Garrigues F, Huwart A *et al.* Localized myofascial inflammation revealed by magnetic resonance imaging in recent-onset polymyalgia rheumatica and effect of tocilizumab therapy. *J Rheumatol* 2019;46:1619–26.
- Wenger M, Schirmer M. Indications for diagnostic use of nuclear medicine in rheumatology: a mini-review. *Front Med (Lausanne)* 2022;9:1026060.
- Blockmans D, de Ceuninck L, Vanderschueren S *et al.* Repetitive 18F-fluorodeoxyglucose positron emission tomography in giant cell arteritis: a prospective study of 35 patients. *Arthritis Rheum* 2006;55:131–7.
- Dasgupta B, Cimmino MA, Kremers HM *et al.* 2012 provisional classification criteria for polymyalgia rheumatica: a European League Against Rheumatism/American College of Rheumatology collaborative initiative. *Arthritis Rheumatol* 2012;64:943–54.
- Mercadante JR, Marappa-Ganeshan R. Anatomy, skin bursa. Treasure Island, FL: StatPearls, 2023. <https://www.ncbi.nlm.nih.gov/books/NBK554438/>.
- Sondag M, Guillot X, Verhoeven F *et al.* Utility of 18F-fluoro-dexoxyglucose positron emission tomography for the diagnosis of polymyalgia rheumatica: a controlled study. *Rheumatology (Oxford)* 2016;55:1452–7.
- Henckaerts L, Gheysens O, Vanderschueren S, Goffin K, Blockmans D. Use of 18F-fluorodeoxyglucose positron emission tomography in the diagnosis of polymyalgia rheumatica-A prospective study of 99 patients. *Rheumatology (Oxford)* 2018;57:1908–16.
- Salvarani C, Barozzi L, Cantini F *et al.* Cervical interspinous bursitis in active polymyalgia rheumatica. *Ann Rheum Dis* 2008;67:758–61.
- Salvarani C, Barozzi L, Boiardi L *et al.* Lumbar interspinous bursitis in active polymyalgia rheumatica. *Clin Exp Rheumatol* 2013; 31:526–31.
- Bywaters EG, Evans S. The lumbar interspinous bursae and Bastrup's syndrome. An autopsy study. *Rheumatol Int* 1982; 2:87–96.
- Bywaters EG. Rheumatoid and other diseases of the cervical interspinous bursae, and changes in the spinous processes. *Ann Rheum Dis* 1982;41:360–70.
- Hatgis J, Granville M, Jacobson RE. Bastrup's disease, interspinous bursitis, and dorsal epidural cysts: radiologic evaluation and impact on treatment options. *Cureus* 2017;9:e1449.
- Cimmino MA, Camellino D, Paparo F *et al.* High frequency of capsular knee involvement in polymyalgia rheumatica/giant cell arteritis patients studied by positron emission tomography. *Rheumatology (Oxford)* 2013;52:1865–72.
- Rehak Z, Sprlakova-Pukova A, Bortlicek Z *et al.* PET/CT imaging in polymyalgia rheumatica: praepubic <sup>18</sup>F-FDG uptake correlates with pectineus and adductor longus muscles enthesitis and with tenosynovitis. *Radiol Oncol* 2017;51:8–14.
- Salvarani C, Cantini F, Macchioni P *et al.* Distal musculoskeletal manifestations in polymyalgia rheumatica: a prospective followup study. *Arthritis Rheumatol* 1998;41:1221–6.
- Marzo-Ortega H, Rhodes LA, Tan AL *et al.* Evidence for a different anatomic basis for joint disease localization in polymyalgia rheumatica in comparison with rheumatoid arthritis. *Arthritis Rheumatol* 2007;56:3496–501.
- Cimmino MA, Parodi M, Zampogna G, Barbieri F, Garlaschi G. Polymyalgia rheumatica is associated with extensor tendon tenosynovitis but not with synovitis of the hands: a magnetic resonance imaging study. *Rheumatology (Oxford)* 2011;50:494–9.
- Cantini F, Salvarani C, Olivieri I *et al.* Remitting seronegative symmetrical synovitis with pitting oedema (RS3PE) syndrome: a prospective follow up and magnetic resonance imaging study. *Ann Rheum Dis* 1999;58:230–6.
- Salvarani C, Pipitone N, Versari A, Hunder GG. Clinical features of polymyalgia rheumatica and giant cell arteritis. *Nat Rev Rheumatol* 2012;8:509–21.
- Hemmig AK, Gozzoli D, Werlen L *et al.* Subclinical giant cell arteritis in new onset polymyalgia rheumatica: a systematic review and meta-analysis of individual patient data. *Semin Arthritis Rheum* 2022;55:152017.
- Meller J, Strutz F, Siefker U *et al.* Early diagnosis and follow-up of aortitis with [<sup>18</sup>F]FDG PET and MRI. *Eur J Nucl Med Mol Imaging* 2003;30:730–6.

34. Prieto-Pena D, Martinez-Rodriguez I, Loricera J *et al.* Predictors of positive <sup>18</sup>F-FDG PET/CT-scan for large vessel vasculitis in patients with persistent polymyalgia rheumatica. *Semin Arthritis Rheum* 2019;48:720–7.
35. van der Geest KSM, Treglia G, Glaudemans A *et al.* Diagnostic value of [18F]FDG-PET/CT in polymyalgia rheumatica: a systematic review and meta-analysis. *Eur J Nucl Med Mol Imaging* 2021;48:1876–89.
36. Moreel L, Boeckxstaens L, Betrains A *et al.* Diagnostic accuracy and validation of <sup>18</sup>F-fluorodeoxyglucose positron emission tomography scores in a large cohort of patients with polymyalgia rheumatica. *Front Med* 2022;9:1026944.
37. Camellino D, Duftner C, Dejaco C. New insights into the role of imaging in polymyalgia rheumatica. *Rheumatology (Oxford)* 2021;60:1016–33.
38. Slart R. FDG-PET/CT(A) imaging in large vessel vasculitis and polymyalgia rheumatica: joint procedural recommendation of the EANM, SNMMI, and the PET Interest Group (PIG), and endorsed by the ASNC. *Eur J Nucl Med Mol Imaging* 2018;45:1250–69.
39. Jamar F, Buscombe J, Chiti A *et al.* EANM/SNMMI guideline for 18F-FDG use in inflammation and infection. *J Nucl Med* 2013;54:647–58.
40. Quinn KA, Rosenblum JS, Rimland CA *et al.* Imaging acquisition technique influences interpretation of positron emission tomography vascular activity in large-vessel vasculitis. *Semin Arthritis Rheum* 2020;50:71–6.
41. Bucierius J, Mani V, Moncrieff C *et al.* Optimizing 18F-FDG PET/CT imaging of vessel wall inflammation: the impact of 18F-FDG circulation time, injected dose, uptake parameters, and fasting blood glucose levels. *Eur J Nucl Med Mol Imaging* 2014;41:369–83.
42. Steinberg JD, Vogel W, Vegt E. Factors influencing brown fat activation in FDG PET/CT: a retrospective analysis of 15,000+ cases. *Br J Radiol* 2017;90:20170093.
43. Huet P, Burg S, Le Guludec D, Hyafil F, Buvat I. Variability and uncertainty of 18F-FDG PET imaging protocols for assessing inflammation in atherosclerosis: suggestions for improvement. *J Nucl Med* 2015;56:552–9.
44. Stellingwerff MD, Brouwer E, Lensen KDF *et al.* Different scoring methods of FDG PET/CT in giant cell arteritis: need for standardization. *Medicine (Baltimore)* 2015;94:e1542.
45. Nielsen BD, Gormsen LC, Hansen IT *et al.* Three days of high-dose glucocorticoid treatment attenuates large-vessel 18F-FDG uptake in large-vessel giant cell arteritis but with a limited impact on diagnostic accuracy. *Eur J Nuclear Med Mol Imaging* 2018;45:1119–28.